

HYDROGEN STORAGE PROPERTIES OF MECHANICALLY ALLOYED Ti-V-MN BODY-CENTERED-CUBIC ALLOYS

Mateusz Balcerzak

Poznań University of Technology, Institute of Materials Science and Engineering, Jana Pawla II no 24, 61-138 Poznan, Poland
Corresponding author: Mateusz Balcerza, e-mail: mateusz.balcerzak@put.poznan.pl

REFERENCE NO	ABSTRACT
HYST-01	$Ti_{0.5}V_{1.5-x}Mn_x$ ($x = 0, 0.1, 0.2, 0.3$) alloys are synthesized by mechanical alloying method, and the effect of Mn content on structure and hydrogenation properties are investigated systematically. All samples are composed of a major body-centered-cubic (BCC) phase. Mn-containing materials consist also a second BCC phase which abundance increases with increase of Mn content in the alloy. Moreover, as Mn content increases, the lattice parameters of both phases decrease. It is presented that all alloys need to be activated before performing the best hydrogenation properties. As the Mn content in Ti-V-Mn alloys increases, the maximum hydrogen storage capacity at room temperature increases first and then decreases. Reversibility of hydriding-dehydriding process is improved after chemical modification of Ti-V alloy.

Keywords:
Ti-V-Mn alloys, mechanical alloying, metal hydrides, hydrogen storage

1. INTRODUCTION

Metal hydrides can store hydrogen in their solid state. For some of them a hydrogen sorption and desorption can be performed at reasonable temperature and pressure (near to ambient). Among many known materials, body-centered-cubic (BCC) solid solutions are considered one of the promising hydrogen storage alloys. It is due to hydrogen storage density which is higher than for well known intermetallic compounds [1,2]. BCC alloys show a total hydrogen storage capacity of $H/M \sim 2$. Unfortunately, they are able to desorb just a half of absorbed hydrogen (at ambient conditions) due to low desorption pressure of monohydride phase [3,4]. Moreover, the use of BCC alloys is limited according to low gravimetric storage density, high hydride stability and poor cyclic stability [3]. Hydrogenation properties of BCC alloys can be improved by use of other production methods, heat-treatment and chemical modification [5,6].

In present study, an effect of partial substitution of V by Mn atoms in $Ti_{0.5}V_{1.5}$ alloy on structure and hydrogen storage properties was investigated. Addition of Mn can increase the effective hydrogen capacity by increasing the plateau pressure and strengthens the anti-oxidation and anti-

corrosion abilities of modified alloy. Mn is also an effective element improving the electrochemical properties of Laves phase alloys for electrode materials of a Ni-MH secondary batteries [7]. Moreover, V-rich BCC alloys suffer from high price of V. Reduction of alloy price can be done by substitution of expensive V atoms by cheaper Mn atoms.

Recently, the present author has reported on the hydrogen storage properties of Ti-V BCC alloy synthesized for the first time by mechanical alloying (MA) method. Obtained nanocrystalline MA BCC alloys were characterized by good activation properties and fast hydrogen sorption [8]. Ball milling was also used in the past to produce composite material based on microcrystalline Ti-V-Mn-Cr BCC and $LaNi_5$ -type alloys. Synthesized material was characterized by improved activation performance which resulted from created core-shell structure [9]. Moreover, S. Couillaud et al. and J. Huot et al. ball milled BCC alloys in order to improve hydrogenation properties of arc melted Ti-V-Mn alloy [4,10].

However, there are no data on nanocrystalline Ti-V-Mn BCC alloys synthesized by MA method. Moreover, in the past Ti-V-Mn alloys were studied as Laves phase related BCC

alloys and there is no information on the structural and hydrogen storage properties of simple Ti-V-Mn BCC alloys [2,6,7,10-14]. For this reason, this work was aimed on studies of structural characterization and hydrogenation properties of MA $Ti_{0.5}V_{1.5-x}Mn_x$ alloys ($x = 0, 0.1, 0.2, 0.3$).

2. EXPERIMENTAL PROCEDURE

Samples of $Ti_{0.5}V_{1.5-x}Mn_x$ alloys ($x = 0, 0.1, 0.2, 0.3$) were prepared by MA the constituent metals under argon atmosphere (99.5% powder Ti, 99.5% powder V, 99.95% powder Mn). MA was continued for 14h to obtain BCC alloys. Details about MA process were included in previous work [8].

The microstructure and chemical compositions were examined by scanning electron microscopy (SEM) with an energy dispersive X-ray spectrometer (EDS) – Tescan VEGA TS5135. Micrographs were used to make particle size dimension distribution histograms. High resolution transmission electron microscope (HRTEM) – Joel ARM 200 F was used to observe microstructure in details. The crystal structure and lattice parameters of MA alloys were determined by X-ray powder diffraction (XRD) using $Cu K\alpha$ radiation – Panalytical Empyrean. XRD measurements were also performed on fully hydrogenated BCC alloys. Diffraction profiles were analyzed by Rietveld refinement Maud program. Williamson-Hall style plot was used to evaluate average crystallite size and lattice strain of MA alloys.

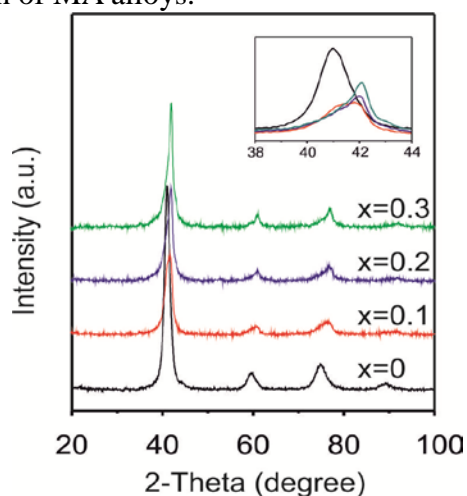


Fig. 1 XRD patterns of MA $Ti_{0.5}V_{1.5-x}Mn_x$ alloys

Table 1 Structural parameters obtained from the Rietveld refinement of Ti-V-Mn X-ray diffraction data.

Sample	Phase	a (Å)	V (Å ³)	P _{abund} (wt%)
$Ti_{0.5}V_{1.5}$ R _{wp} =4.11 S=1.17	BCC	3.1066	29.9817	100
$Ti_{0.5}V_{1.4}Mn_{0.1}$ R _{wp} =8.08 S=1.48	BCC	3.0843	29.3407	95.12
	BCC	3.0469	28.2862	4.88
$Ti_{0.5}V_{1.3}Mn_{0.2}$ R _{wp} =6.05 S=1.21	BCC	3.0795	29.2039	84.23
	BCC	3.0421	28.1527	15.77
$Ti_{0.5}V_{1.2}Mn_{0.3}$ R _{wp} =5.91 S=1.29	BCC	3.0693	28.9147	58.38
	BCC	3.0373	28.0197	41.62

P_{abund} - phase abundance

Hydrogen sorption/desorption behaviour of $Ti_{0.5}V_{1.5-x}Mn_x$ alloys was characterized at near room temperature by kinetic/activation curves and pressure-composition isotherms (PCI). They were measured by a Sieverts-type device – a product of Particulate Systems. Details concerning these studied were included in previous work [8]. Differential scanning calorimetry (DSC) studies were made on fully hydrogenated samples under argon protective gas with a constant heating rate of 10K/min – TA DSC Q20.

3. RESULTS AND DISCUSSION

3.1. Microstructure, structure and phase composition

Chemical composition of unmodified, Ti-V alloy was chosen based on data from previous work - $Ti_{0.5}V_{1.5}$ alloy was found to perform lowest hydride decomposition temperature [8].

Characterization of MA alloys was started using a XRD method. XRD patterns of $Ti_{0.5}V_{1.5-x}Mn_x$ alloys ball milled for 14h are shown in Fig. 1. All of studied alloys are composed of main BCC structure (Im-3m space group). Moreover, in modified Ti-V-Mn alloys a minor phase characterized by the same BCC structure was detected. The lattice parameter of minor phase is smaller than of

main phase. The coexistence of two BCC phases is clearly visible in inset of Fig. 1 where (110) peaks of both phases are

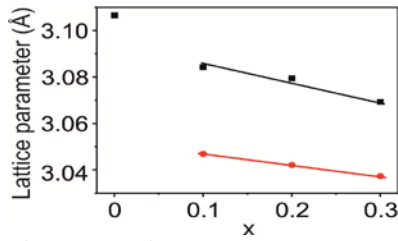


Fig. 2 Lattice parameter as a function of x in $Ti_{0.5}V_{1.5-x}Mn_x$ alloys (black squares refer to BCC main phase, red dots refer to BCC minor phase)

overlapped. Moreover, it is worth noting that Mn peaks which possess BCC structure in room temperature (I-43m space group) were not detected on XRD patterns. It means that Mn can be easily incorporated into BCC phase [15].

The phase abundance of minor BCC phase is increasing with increase of Mn content in the alloy to reach 41.62 wt.% for $Ti_{0.5}V_{1.2}Mn_{0.3}$ alloy (Table 1).

Since V and Mn elements have different atomic sizes, chemical composition is considered to affect the alloys lattice parameters. As expected, peaks positions (corresponded to both BCC phases) are shifted toward higher angles while Mn element content in studied $Ti_{0.5}V_{1.5-x}Mn_x$ alloys is increasing. This implies decrease of unit cell volume.

Fig. 2 shows a variation of lattice parameters of $Ti_{0.5}V_{1.5-x}Mn_x$ alloys with increase of substitution, which clearly shows the effect of chemical modification on lattice parameters. Lattice parameters were obtained from

Table 2 Average particle size, crystallites size and lattice strain of obtained alloys.

Sample	Average size of particle (μm)	Crystallites size (nm)	Lattice strain (%)
$Ti_{0.5}V_{1.5}$	14.6	5.4	1.1
$Ti_{0.5}V_{1.4}Mn_{0.1}$	18.0	3.8	2.0
$Ti_{0.5}V_{1.3}Mn_{0.2}$	7.4	3.2	2.4
$Ti_{0.5}V_{1.2}Mn_{0.3}$	4.5	5.6	1.4

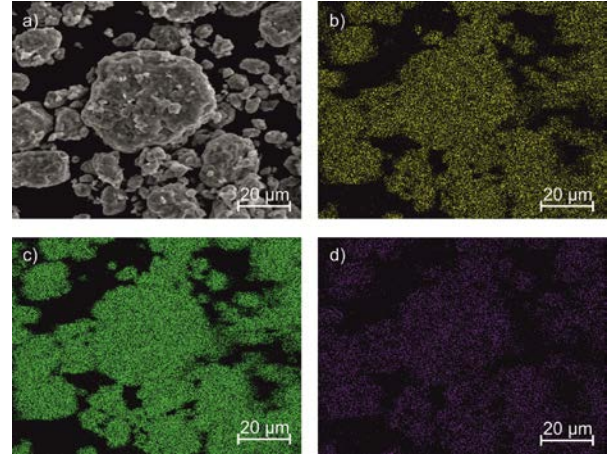


Fig. 3 SEM micrograph of $Ti_{0.5}V_{1.2}Mn_{0.3}$ (a), corresponding EDS elements maps of Ti K α (b), V K α (c), Mn K α (d)

Rietveld refinement method (Table 1). The lattice parameter decreased linearly with increasing Mn in Mn-containing alloys. This is attributed to atomic size effect: the Goldschmidt radii for V and Mn are 0.135 and 0.112(α)~0.137(γ) nm, respectively [16]. As can be seen from Fig. 2 Mn introduced dissolves slightly more in the main BCC phase than in the minor BCC phase.

The same tendency was noticed for Laves phase related BCC alloys for which lattice parameters of both phases (BCC and Laves) decreased with increasing Mn content [7].

XRD data was used to determine average

Table 3 Chemical composition of samples determined from materials weighted before synthesis and from EDS measurements.

Sample	E	W_{syn} (%)	W_{EDS} (%)	Formula obtained from EDS
$Ti_{0.5}V_{1.5}$	Ti	23.88	24.86	$Ti_{0.5}V_{1.42}$
	V	76.12	75.14	
$Ti_{0.5}V_{1.4}Mn_{0.1}$	Ti	23.79	24.62	$Ti_{0.5}V_{1.34}Mn_{0.09}$
	V	70.76	70.38	
	Mn	5.45	5.00	
$Ti_{0.5}V_{1.3}Mn_{0.2}$	Ti	23.69	25.59	$Ti_{0.5}V_{1.21}Mn_{0.15}$
	V	65.45	65.73	
	Mn	10.86	8.68	
$Ti_{0.5}V_{1.2}Mn_{0.3}$	Ti	23.60	26.93	$Ti_{0.5}V_{1.04}Mn_{0.22}$
	V	60.18	59.68	
	Mn	16.22	13.39	

E - element

W_{syn} - weight before synthesis

W_{EDS} - weight based on EDS (%)

crystallite size and lattice strain (Table 2). There is no tendency of crystallite size and lattice strain changes with increasing of Mn concentration in the alloy.

EDS mappings of $Ti_{0.5}V_{1.2}Mn_{0.3}$ are shown in Fig. 3. All elements are homogeneously distributed throughout all synthesized and studied BCC alloy. The average elemental compositions of all studied BCC alloys are listed in Table 3. EDS data shows that chemical compositions of obtained alloys are not matching with expected compositions. However, the differences between these compositions are rather small and can be associated with the accuracy of EDS method.

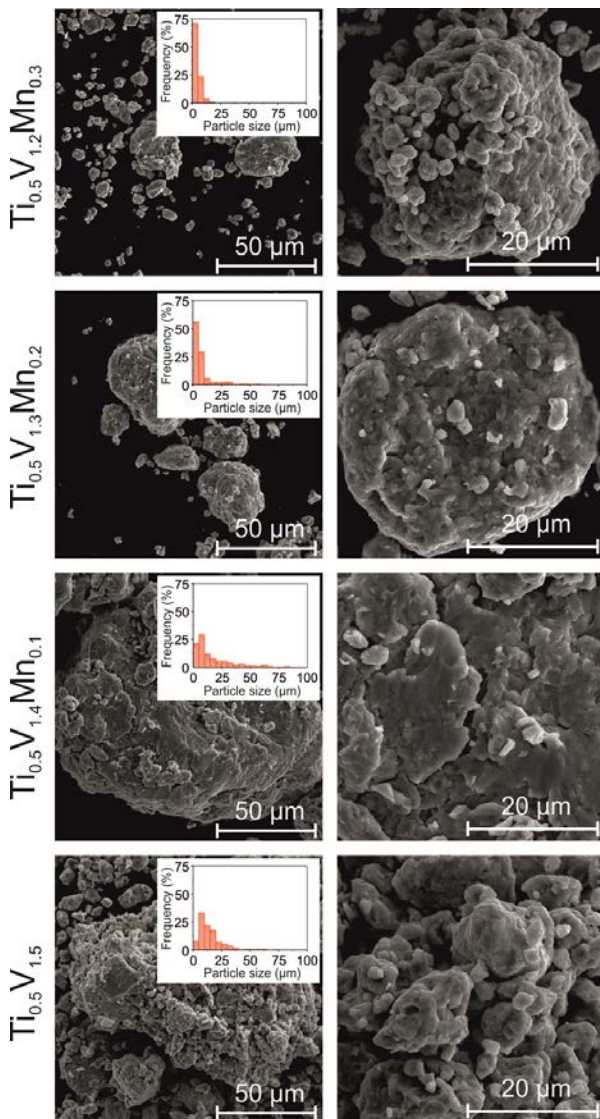


Fig. 4 SEM micrographs at two magnifications and corresponding particle size dimension distribution histograms (insets) of $Ti_{0.5}V_{1.5-x}Mn_x$ alloys

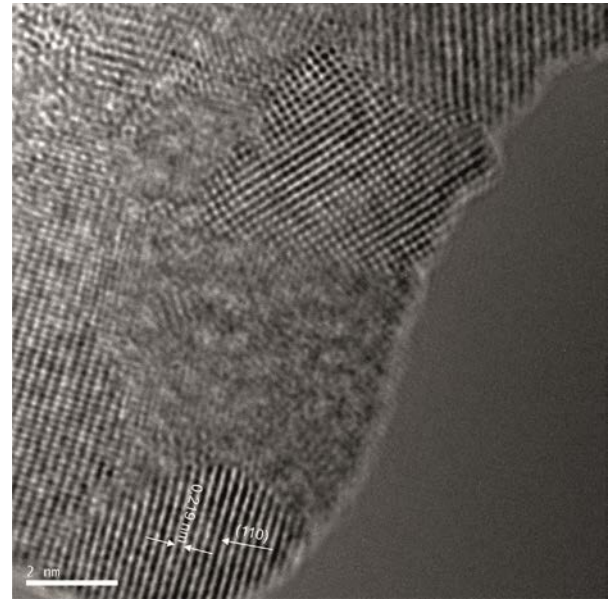


Fig. 5 HRTEM image of $Ti_{0.5}V_{1.4}Mn_{0.1}$ alloy

Fig. 4 shows SEM micrographs (secondary electrons) of $Ti_{0.5}V_{1.5-x}Mn_x$ alloys. Synthesized BCC alloys are made of irregular particles which are characterized by porous, cleavage and fractured morphology. BCC powders particles size distribution shows bimodal character – small grains (size of a few μm) are agglomerated in much bigger forms (from tens to hundred μm).

Based on SEM micrographs, particle size dimension distribution histograms for $Ti_{0.5}V_{1.5-x}Mn_x$ alloys were made (insets of Fig. 4). Moreover, in Table 2 presented are average particle sizes of BCC alloys. It is easy to see that partial substitution of V by Mn atoms resulted firstly in increase of average particle size - from 14.6 μm for $Ti_{0.5}V_{1.5}$ to 18.0 μm $Ti_{0.5}V_{1.4}Mn_{0.1}$. For alloys with higher Mn content a reduction of particle sizes is noticed – to reach 4.5 μm $Ti_{0.5}V_{1.2}Mn_{0.3}$.

Fig. 5 presents a HRTEM image of $Ti_{0.5}V_{1.4}Mn_{0.1}$ alloy – which represents structure of all studied BCC alloys. Ti-V-Mn alloys are characterized by multicrystalline structure – nanocrystals which are oriented in different directions, forms a more complex structures. Crystallites sizes seen on HRTEM images are in the same order of magnitude as values obtained from Williamson-Hall style plot. What is more, the d_{100} spacing value is

similar to value calculated from Rietveld refinement (Fig. 5).

3.2. Hydrogen storage properties

The most meaningful data obtained from hydrogenation - dehydrogenation measurements of synthesized BCC alloys are listed in Table 4. All of Ti-V-Mn alloys were tested without any activation. In Fig. 6 presented are time-capacity curves of $Ti_{0.5}V_{1.5-x}Mn_x$ alloys in activation/kinetic

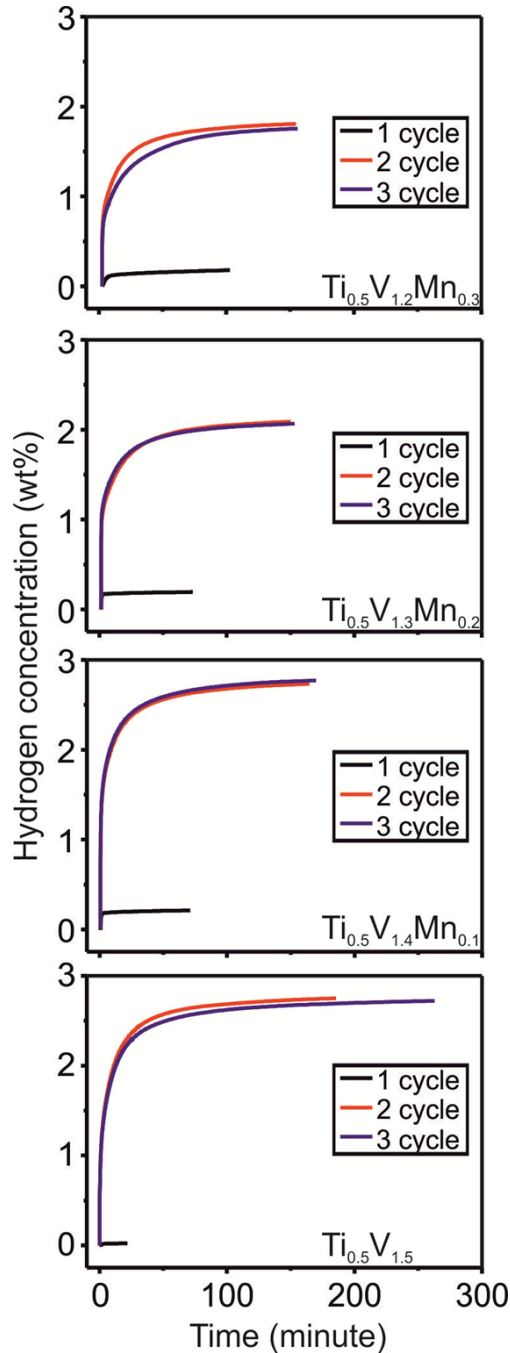


Fig. 6 Time-capacity curves of $Ti_{0.5}V_{1.5-x}Mn_x$ alloys in activation/kinetic measurements

measurements. On each of BCC sample, three activation/kinetic measurements were done. Between the cyclec, samples were degassed at 673 K.

One of main problems concerning application of BCC alloys is difficulty of activation [2]. All of tested samples are in inactive state in the first cycle. The inactive state of studied BCC alloys is most likely associated with an

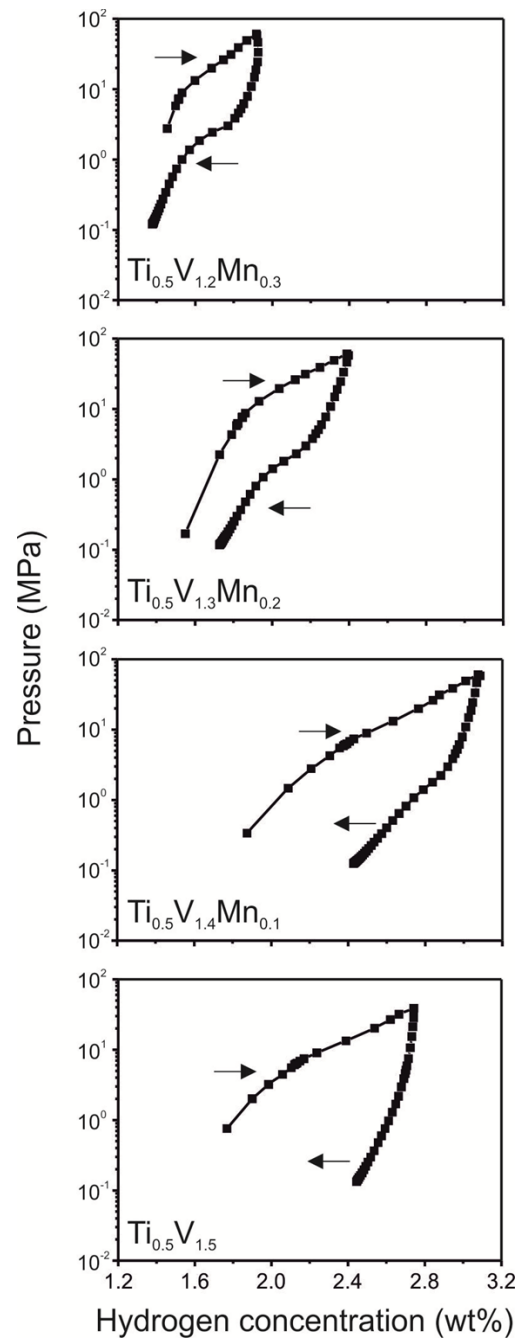


Fig. 7 P-C Isotherms at 303 K of $Ti_{0.5}V_{1.5-x}Mn_x$ alloys. Arrows indicate direction of hydrogen concentration changes (sorption/desorption)

Table 4 Summarized data from PCI and DSC measurements analyses on Ti-V and Ti-V-Mn alloys

Sample	Kinetic measurer				
	A _{cycles}	H (wt%)			1
		1 cycle	2 cycle	3 cycle	
Ti _{0.5} V _{1.5}	2	0.02	2.75	2.72	-
Ti _{0.5} V _{1.4} Mn _{0.1}	3	0.20	2.73	2.76	3
Ti _{0.5} V _{1.3} Mn _{0.2}	3	0.19	2.09	2.07	2
Ti _{0.5} V _{1.2} Mn _{0.3}	2	0.18	1.81	1.75	7

A_{cycles} – number of activation cycles needed to obtain best kinetic properties

H – hydrogen concentration from kinetic measurements

T₉₅ – time needed to reach 95% of maximum hydrogen capacity

R_{H/DH} - reversibility of hydriding-dehydriding process (PCT tests)

T_{H-des} (°C) – hydrogen desorption peak temperature

oxide layer at surface which restrains the hydrogen sorption reaction [17,18].

However, the activation of presented in this paper alloys does not seem to be a problem. All alloys shown the best or nearly the best hydrogenation kinetics after just one cycle of activation (hydrogenation at 3 MPa at 303 K followed by materials degassing at 673 K). Presented activation procedure is shorter than presented in the past for Ti_{1.0}V_{1.1}Mn_{0.9} arc melted alloy for which two cycles of activation were needed (initial hydrogenation at 5 MPa of hydrogen gas, evacuation at 353 K for 1h) [19].

All of studied samples in activated state can absorb hydrogen without any incubation time. The hydrogenation process in the initial phase of reaction is very fast. These results differ much from those obtained by X.B Yu et al. These group reported that Ti-V-Mn-Cr alloy synthesized by magnetic levitation melting method needs 10-30 min (depending on melt-quenching time) to start hydrogen sorption process [20]. The reason could be the differences in microstructure. Hydrogen can diffuse more easily on the grain boundaries in nanocrystalline materials (synthesized in this work) than in microcrystalline alloys.

S.F. Santos et al., who studied Ti-Mn-(FeV) Laves phase related BCC alloys stated that incubation time in BCC alloys could be related to absence of C14 Laves phase [18]. However, studied in this paper materials are not co-created of C14 Laves phase and the incubation time was not observed.

The time needed to absorb 95% of maximum hydrogen capacity by studied BCC alloys does not depend on chemical composition of material. It is 60-67 minutes for all of the alloys.

The maximum hydrogen capacity was reduced from 2.75 wt.% for Ti_{0.5}V_{1.5} alloy to 1.81 wt.% for Ti_{0.5}V_{1.2}Mn_{0.3} alloy. One explanation of the hydrogen storage capacity decrease is the main BCC phase worked as the main hydrogen storage medium and the decrease of the amount of the main phase would decrease the hydrogen storage capacity. However, the secondary phase, can also react reversibly with hydrogen. Therefore, the increase of the amount of secondary phase can not be taken as sole reason for the decrease in the maximum hydrogen desorption capacity. Therefore, the decrease in maximum hydrogen storage capacity is most likely attributed to the increase of plateau equilibrium pressure which is caused by decrease of the hydrogen stability in the lattice states due to the decrease of the lattice parameters.

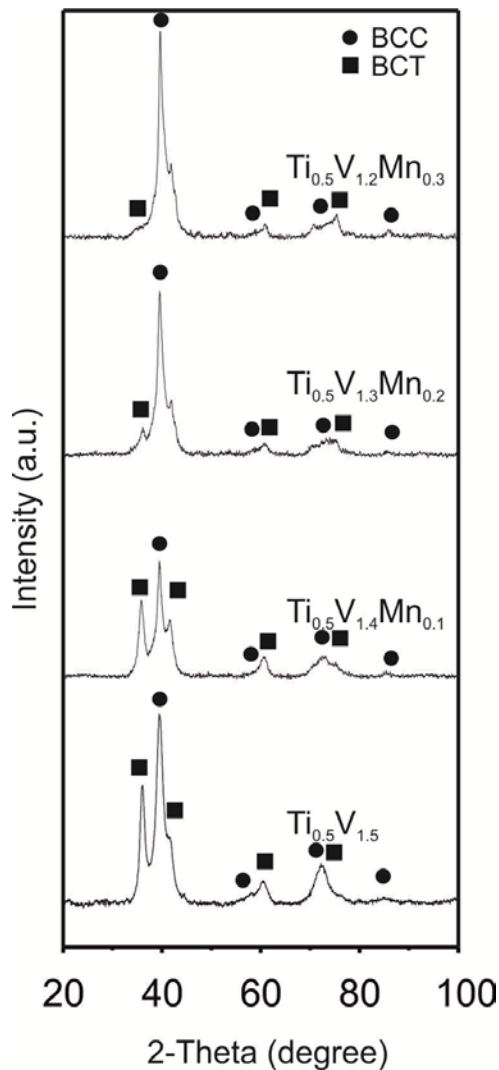


Fig. 8 XRD patterns of fully hydrogenated $Ti_{0.5}V_{1.5-x}Mn_x$ alloys

Maximum hydrogen storage capacities of studied $Ti_{0.5}V_{1.5-x}Mn_x$ alloys are much higher than these obtained for arc melted Ti-V-Mn Laves phase related BCC alloys. The unambiguous indication reason of this difference is impossible based on the available data. This may be due to different chemical composition, phase composition, microstructure [13,14].

P-C isotherms received for studied BCC alloys at 303 K are presented in Fig. 7. On these curves visible are one plateau regions which are characterized by large slope. Equilibrium plateau slope is undesirable for application of metal hydrides. To make plateau region more flat, heat treatment which

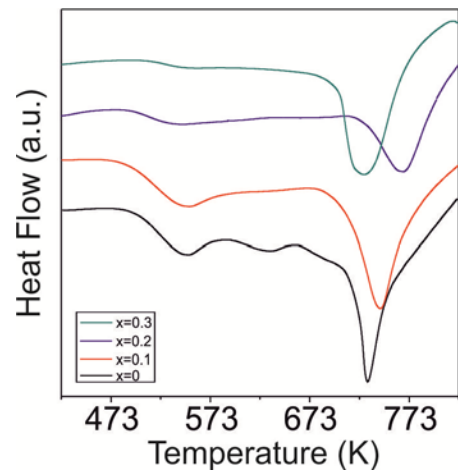


Fig. 9 DSC profiles of $Ti_{0.5}V_{1.5-x}Mn_x$ alloys

hydrides can make material more homogenous can be done [22].

As wrote C.Y. Seo et al. Mn is considered to be effective element in decreasing the slope of the plateau pressure [21]. However, in this work an opposite tendency was observed - the slope increased with increasing Mn content in BCC alloys.

Visible on P-C isotherms plateau region corresponds most likely to two-phase region of the hydrogenated solid-solution phase (distorted BCC) and BCT hydride phase. Moreover, it is important to note that there may be another plateau below the pressure range contributed to irreversible hydrogen storage within the current PCT measuring range [10].

Equilibrium pressure and width of plateau depended on BCC alloys chemical composition. Increasing Mn content made the plateau narrower, increase the equilibrium pressure and decrease the hydrogen sorption/desorption hysteresis. Increase of plateau pressure (resulted from mentioned decrease of unit cell) caused less hydride stability which results in easier hydrogen desorption.

A hydrogen desorption properties of tested BCC alloys are quantitatively presented by reversibility of hydriding-dehydriding process (Table 4). Only about 11% of hydrogen absorbed in $Ti_{0.5}V_{1.5}$ alloy can be easily desorbed in ambient conditions. The reversibility was improved by chemical modification of BCC alloys by Mn atoms and reached 28% for $Ti_{0.5}V_{1.3}Mn_{0.2}$ and

Ti_{0.5}V_{1.2}Mn_{0.3} alloys. This amount is, however, not enough for practical applications.

After hydrogen sorption-desorption studies, XRD and DSC measurements were done on activated, fully hydrogenated Ti_{0.5}V_{1.5-x}Mn_x alloys. From the literature it is well known that absorption and desorption of hydrogen in BCC alloys occurs through three steps [3,23]:

- firstly when hydrogen is applied, BCC alloy form a solid solution hydride phase (hydrogen atoms randomly occupy octahedral interstitial sites of BCC metal lattice. Maximum hydrogen capacity of this solid solution is 1.5 wt.%. Hydrogen desorption from this hydride is impossible in ambient conditions,

- while the hydrogen pressure increases, hydrogen atoms start to occupy octahedral sites in ordered way, creating monohydride phase with body-centered-tetragonal (BCT) structure (I₄/mmm space group). This phase corresponds to BCC structure elongated along c axis. The BCT hydrogen maximum uptake is 1.9 wt.%.

- finally, further increase in hydrogen pressure causes filling of tetrahedral interstitial sites and formation of dihydride phase characterized by face-centered-cubic (FCC) structure (Fm-3m space group). The FCC hydrogen maximum uptake is 4 wt.%. It is worth noting that Ti and V metals are known to form a hydride with FCC structure and Mn is a hydride non-forming element [19].

XRD patterns of studied BCC alloys in hydrogenated state are presented in Fig. 8. All of hydrides are composed of two phases: distorted BCC phase (α -phase) and BCT phase. The BCT phase abundance decreased with increase of Mn in studied BCC alloys – from 32.3% for unmodified Ti_{0.5}V_{1.5} to 4.4% for Ti_{0.5}V_{1.2}Mn_{0.3} alloy. The XRD data of hydrogenated samples fit well to presented in Table 4 maximum hydrogen concentrations. Nevertheless, hydrogen concentration obtained for Ti_{0.5}V_{1.5} and Ti_{0.5}V_{1.4}Mn_{0.1} greatly exceeds the maximum hydrogen capacity of BCT phase. It suggests that both of materials are also partially composed of

FCC phase which can not be detected due to low content of the hydride phase.

To understand the desorption behavior of tested BCC alloys, DSC studies were performed on fully hydrogenated Ti_{0.5}V_{1.5-x}Mn_x alloys. DSC profiles obtained with heating rate of 10 K/min in an argon atmosphere are shown in Fig. 9. The hydrides decomposition temperatures are listed in Table 4. The desorption temperatures found in this work are not the exact one, due to air poisoning of alloys during transferring of BCC powder from glove box to DSC device. However, the stability of hydrides phases can be compared quite well.

Ti_{0.5}V_{1.5} and Ti_{0.5}V_{1.4}Mn_{0.1} DSC curves have three endothermic peaks accounting for three phase transformations in the regions 532-551K, 631-638K and 716-744K, respectively. The first, low temperature hydride decomposition reaction is associated most probably with phase transformation from FCC to BCT phase. Next, the BCT decomposes to hydrogenated BCC phase. At last, the high temperature peak is associated with decomposition of hydrogenated BCC phase to dehydrogenated BCC phase. Described hydride decomposition process which consists of three steps proves the presence of additional to BCC and BCT hydride phase. This is most likely the dihydride FCC phase.

For Ti_{0.5}V_{1.3}Mn_{0.2} and Ti_{0.5}V_{1.2}Mn_{0.3} alloys only two endothermic peaks are visible. The BCC dehydrogenation temperature is firstly increased and then decreased with increase of Mn content in BCC alloy. However, the lowest BCC hydride decomposition was obtained for unmodified Ti-V alloy. The dehydrogenation temperatures are high which indicates high thermal stability of hydride phases. The hydride decomposition temperature must be lowered in order to consider BCC alloys as hydrogen storage systems.

The enthalpy of dehydrogenation process reached 240.3, 200.3, 85.5 and 131.6 J/g respectively for x=0, 0.1, 0.2 and 0.3. The decrease of enthalpy with increment of Mn content implies that Mn is effective in reducing the stability of BCC hydride phase.

It should be noticed, that studied $Ti_{0.5}V_{1.5-x}Mn_x$ and additionally synthesized $Ti_{0.5}V_{1.4-x}Ni_{0.1}Mn_x$ alloys have been also tested for their usefulness as negative electrodes in Ni-MH_x secondary electrodes. The electrochemical tests results are not shown in this work because increasing Mn content does not improve the electrochemical properties. The same conclusion was also reported by Q.A. Zhang et al. for Laves phase related BCC alloys [7].

4. CONCLUSIONS

Based on studies of structure, microstructure, hydrides thermal stability and hydrogenation/dehydrogenation properties of BCC alloys, the effect of Mn content on hydrogen storage properties of nanocrystalline $Ti_{0.5}V_{1.5-x}Mn_x$ were investigated in present work. The obtained results are summarized as follows:

- partial substitution of V by Mn atoms resulted in creation of minor BCC phase which phase abundance increases with increase of Mn content in the alloy,
- hydrogenation - dehydrogenation properties of BCC alloys result from chemical composition and lattice parameters. Maximum hydrogen storage capacity was reduced with increase of Mn content in the alloy. The reason of this phenomenon is reduction of cell volumes of BCC phases,
- chemical modification by Mn atoms improves the reversibility of hydriding/dehydriding process.

1. Acknowledgements

Financial assistance from National Science Centre, Poland (no. 2015/17/N/ST8/00271)

References

- [1] X.B. Yu, S.L. Feng, Z. Wu, B.J. Xia, N.X. Xu, Hydrogen storage performance of Ti-V-based BCC phase alloys with various Fe content, *Journal of Alloys and Compounds*, Vol. 393, 2005, pp.129-134
- [2] X.B. Yu, Z. Wu, B.J. Xia, N.X. Xu, Enhancement of hydrogen storage capacity of Ti-V-Cr-Mn BCC phase alloys, *Journal of*

Alloys and Compounds, Vol. 372, 2004, pp.272-277

- [3] H. Kim, K. Sakaki, Y. Nakamura, Improving the cyclic stability of V-Ti-Mn bcc alloys using interstitial elements, *Materials Transactions*, Vol. 55, 2014, pp.1144-1148
- [4] S. Couillaud, H. Enoki, S. Amira, J.L. Bobet, E. Akiba, J. Huot, Effect of ball milling and cold rolling on hydrogen storage properties of nanocrystalline TiV1.6Mn0.4 alloy, *Journal of Alloys and Compounds*, Vol. 484, 2009, pp.154-158
- [5] A. Kumar, K. Shashikala, S. Banerjee, J. Nuwad, P. Das, C.G.S. Pillai, Effect of cycling on hydrogen storage properties of Ti2CrV alloy, *International Journal of Hydrogen Energy*, Vol. 37, 2012, pp.3677-3682
- [6] H.Y. Zhou, F. Wang, J. Wang, Z.M. Wang, Q.R. Yao, J.Q. Deng, C.Y. Tang, G.H. Rao, Hydrogen storage properties and thermal stability of V35Ti20Cr45 alloy by heat treatment, *International Journal of Hydrogen Energy*, Vol. 39, 2014, pp.14887-14895
- [7] Q.A. Zhang, Y.Q. Lei, X.G. Yang, Y.L. Du, Q.D. Wang, Influence of Mn on phase structure and electrochemical properties of V3TiNi0.56Hf0.24 alloy, *International Journal of Hydrogen Energy*, Vol. 25, 2000, pp.657-661
- [8] M. Balcerzak, Structure and hydrogen storage properties of mechanically alloyed Ti-V alloys, *International Journal of Hydrogen Energy*, Vol. 42, 2017, pp.23698-23707
- [9] X.B. Yu, Z. Wu, B.J. Xia, N.X. Xu, Improvement of activation performance of the quenched Ti-V-based BCC phase alloys, *Journal of Alloys and Compounds*, Vol. 386, 2005, pp.258-260
- [10] J. Huot, H. Enoki, E. Akiba, Synthesis, phase transformation, and hydrogen storage properties of ball-milled TiV0.9Mn1.1, *Journal of Alloys and Compounds*, Vol. 453, 2008, pp.203-209
- [11] K. Young, T. Ouchi, J. Nei, T. Meng, Effects of Cr, Zr, V, Mn, Fe, and Co to the hydride properties of Laves phase-related body-centered-cubic solid solution alloys, *Journal of Power Sources*, Vol. 281, 2015, pp.164-172

- [12] J.H. Yoo, G. Shim, C.N. Park, W.B. Kim, S.W. Cho, Influence of Mn or Mn plus Fe on the hydrogen storage properties of the Ti-Cr-V alloy, *International Journal of Hydrogen Energy*, Vol. 34, 2009, pp.9116-9121
- [13] L. Pickering, J. Li, D. Reed, A.I. Bevan, D. Book, Ti-V-Mn based metal hydrides for hydrogen storage, *Journal of Alloys and Compounds*, Vol. 580, 2013, pp.S233-S237
- [14] M. Shibuya, J. Nakamura, E. Akiba, Hydrogenation properties and microstructure of Ti-Mn-based alloys for hybrid hydrogen storage vessel, *Journal of Alloys and Compounds*, Vol. 466, 2008, pp.558-562
- [15] C.Y. Seo, J.H. Kim, P.S. Lee, J.Y. Lee, Hydrogen storage properties of vanadium-based b.c.c. solid solution metal hydrides, *Journal of Alloys and Compounds*, Vol. 348, 2003, pp.252-257
- [16] Y. Nakamura, E. Akiba, Hydriding properties and crystal structure of NaCl-type mono-hydrides formed from Ti-V-Mn BCC solid solutions, *Journal of Alloys and Compounds*, Vol. 345, 2002, pp.175-182
- [17] S. Challet, M. Latroche, F. Heurtaux, Hydrogenation properties and crystal structure of the single BCC (Ti_{0.355}V_{0.645})_{100-x}M_x alloys with M = Mn, Fe, o, Ni (x = 7, 14 and 21), *Journal of Alloys and Compounds*, Vol. 439, 2007, pp.294-301
- [18] X.B. Yu, Z. Wu, B.J. Xia, N.X. Xu, The activation mechanism of Ti-V-based hydrogen storage alloys, *Journal of Alloys and Compounds*, Vol. 375, 2004, pp.221-223
- [19] Y. Nakamura, E. Akika, New hydride phase with a deformed FCC structure in the Ti-V-Mn solid solution-hydrogen system, *Journal of Alloys and Compounds*, Vol. 311, 2000, pp.317-321
- [20] X.B. Yu, Z. Wu, N.X. Xu, Effect of melt-quenching rates on the hydrogen storage properties of Ti-based BCC alloy, *Physica B*, Vol. 344, 2004, pp.456-461
- [21] S.F. Santos, J. Huot, Hydrogenation storage in Ti-Mn-(FeV) BCC alloy, *Journal of Alloys and Compounds*, Vol. 480, 2009, pp.5-8
- [22] X.B. Yu, Z. Wu, N.X. Xu, Effect of melt-quenching rates on the hydrogen storage properties of Ti-based BCC phase alloy, *Physica B*, Vol. 344, 2004, pp.456-461
- [23] Y. Nakamura, K. Oikawa, T. Kamiyama, E. Akiba, Crystal structure of two hydrides formed from a Ti-V-Mn BCC solid solution alloy studied by time-of-flight neutron powder diffraction – a NaCl structure and CaF₂ structure, *Journal of Alloys and Compounds*, Vol. 316, 2001, pp.284-289